

# MaskingDepth: Masked Consistency Regularization for Semi-supervised Monocular Depth Estimation

Jongbeom Baek<sup>1\*</sup> Gyeongnyeon Kim<sup>1\*</sup> Seonghoon Park<sup>1\*</sup> Honggyu An<sup>1</sup>

Matteo Poggi<sup>2</sup> Seungryong Kim<sup>1†</sup>

<sup>1</sup>Korea University, Seoul, Korea <sup>2</sup>University of Bologna, Bologna, Italy

{baem0911, kkn9975, seong0905, hg010303, seungryong.kim}@korea.ac.kr m.poggi@unibo.it

## Abstract

We propose *MaskingDepth*, a novel semi-supervised learning framework for monocular depth estimation to mitigate the reliance on large ground-truth depth quantities. *MaskingDepth* is designed to enforce consistency between the strongly-augmented unlabeled data and the pseudo-labels derived from weakly-augmented unlabeled data, which enables learning depth without supervision. In this framework, a novel data augmentation is proposed to take the advantage of a naïve masking strategy as an augmentation, while avoiding its scale ambiguity problem between depths from weakly- and strongly-augmented branches and risk of missing small-scale instances. To only retain high-confident depth predictions from the weakly-augmented branch as pseudo-labels, we also present an uncertainty estimation technique, which is used to define robust consistency regularization. Experiments on KITTI and NYU-Depth-v2 datasets demonstrate the effectiveness of each component, its robustness to the use of fewer depth-annotated images, and superior performance compared to other state-of-the-art semi-supervised methods for monocular depth estimation. Furthermore, we show our method can be easily extended to domain adaptation task. Our code is available at <https://github.com/KU-CVLAB/MaskingDepth>.

## 1. Introduction

Monocular depth estimation, aiming to predict a dense depth map from a single image, has been one of the most essential tasks in numerous applications, such as augmented reality (AR) [41], virtual reality (VR) [30], and autonomous driving [70, 36].

As a pioneering work, Eigen et al. [16] first introduced a deep learning-based approach for this task, and several

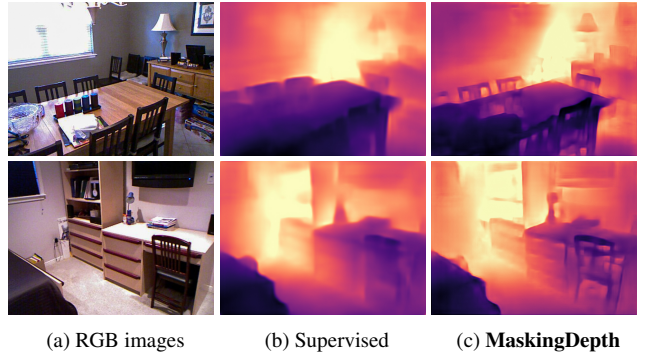


Figure 1. **Qualitative results of MaskingDepth:** Our proposed MaskingDepth produces high quality depth maps by leveraging a large amount of unlabeled data.

works [42, 34, 60, 44, 15, 17, 40, 52, 51] have achieved higher accuracy throughout the years. These methods are mostly formulated in a supervised learning regime, which requires a large number of images and corresponding ground-truth depths. These are notoriously challenging to obtain [20, 54] compared to other types of annotation, such as image class labels [55] and segmentation labels [75]. To overcome this problem, self-supervised learning techniques [74, 23, 24] have emerged, which formulate monocular depth estimation as an image reconstruction problem. Although this strategy seems to be an attractive solution, these methods often require extra data, such as stereo pairs or video sequences which are not always available [74, 23, 24]. In addition, they are known to often generate blurred depth at object boundaries [7, 3].

On the other hand, semi-supervised learning approaches using stereo-based knowledge distillation [57, 6, 7] have been proposed. However, they are constrained by the need for stereo image pairs and additional computation costs for training a stereo model. Moreover, some works [38, 1] have attempted to simply combine supervised learning and reconstruction-based self-supervised learning [74, 23, 24], but they directly inherit of limitations of existing self-

\*Equal contribution

†Corresponding author

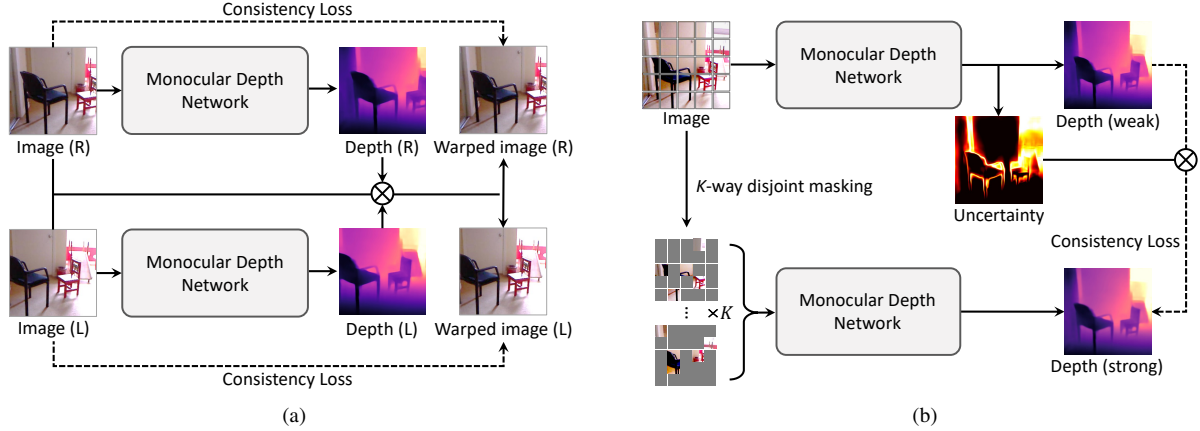


Figure 2. **Motivation:** (a) existing self-supervised methods [24, 19, 23] that enforce consistency between one image and another warped image from stereo or sequential frames, which often results in blurred artifacts at object boundaries, and (b) our framework that uses uncertainty-aware consistency regularization by adopting  $K$ -way disjoint masking for augmentation, which shows highly improved performance with sparse depth data in a semi-supervised learning setting.

supervised learning methods.

In this paper, for the first time, we present a novel semi-supervised learning framework, called MaskingDepth, for monocular depth estimation based on an uncertainty-aware consistency regularization. Our framework enforces consistency between strongly-augmented unlabeled data and pseudo-labels obtained from weakly-augmented unlabeled data. To apply enough perturbations to an input image, we propose a new data augmentation, called  $K$ -way disjoint masking, inspired by recent masked image modeling strategies for vision Transformers [4, 66, 29]. The naïve masking technique [4, 66, 29] yielded superior performance on classification tasks such as image classification and semantic segmentation. However, adopting this to monocular depth estimation, which heavily relies on context information to estimate the depth, may cause scale ambiguity and omit the context of small objects [29]. To overcome this, the  $K$ -way disjoint masking jointly decodes scattered tokens that are encoded from a  $K$ -disjoint set of tokens independently, and thus mitigates the scale ambiguity and restores the full context from the image while retaining the benefits of masking-based data augmentation. In our framework, we encourage depth and feature consistencies [4] across two branches from two augmented views by  $K$ -way disjoint masking. In addition, we propose an uncertainty estimation technique [32, 50] to aid depth consistency and facilitate convergence by filtering out the noise of pseudo labels.

In the experiments, we evaluate MaskingDepth on standard benchmarks, including KITTI [20] and NYU-Depth-v2 [54], showing outstanding performance compared to previous methods. We validate each component through an extensive ablation study and demonstrate that our approach can be easily used for domain adaptation.

## 2. Related Work

**Monocular depth estimation.** Monocular depth estimation aims at estimating a depth from a single image. [16] pioneering work tackled this task with deep neural networks. Since then, several approaches [42, 60] based on supervised learning, i.e., utilizing ground-truth labels, have been presented to improve performance. Although these methods have achieved remarkable accuracy over traditional, hand-crafted approaches [53, 39], their success depends on massive amounts of ground-truth depth maps that require a labor-intensive process for collection and cleaning [20, 54].

To address this limitation, self-supervised learning methods [65, 19, 24] formulate the task as an image reconstruction, leveraging geometric information over stereo pairs or a sequence of frames. These approaches have emphasized the importance to mitigate the dependency on annotations. However, they often produces indistinct depth result near object boundaries and disregards occluded pixels [7]. Unlike both of the aforementioned approaches, there has not been much work on semi-supervised depth estimation. [38] simply combined supervised and self-supervised loss functions and [1] utilized a left-right consistency to improve performance. Recently, several works [28, 6, 58, 63, 7] have attempted to use stereo knowledge to distill labels for monocular depth estimation. However, they are still constrained by the need for specific data (stereo pairs) and additional computation cost (training a stereo module). Our proposed framework alleviates the reliance on labeled data by leveraging consistency regularization which allows us to use unlabeled data.

**Masked image modeling.** Masked image modeling is the process of learning representations by reconstructing images that are corrupted by masking [66, 29, 4]. After BERT [10] proposed the masked language modeling task,

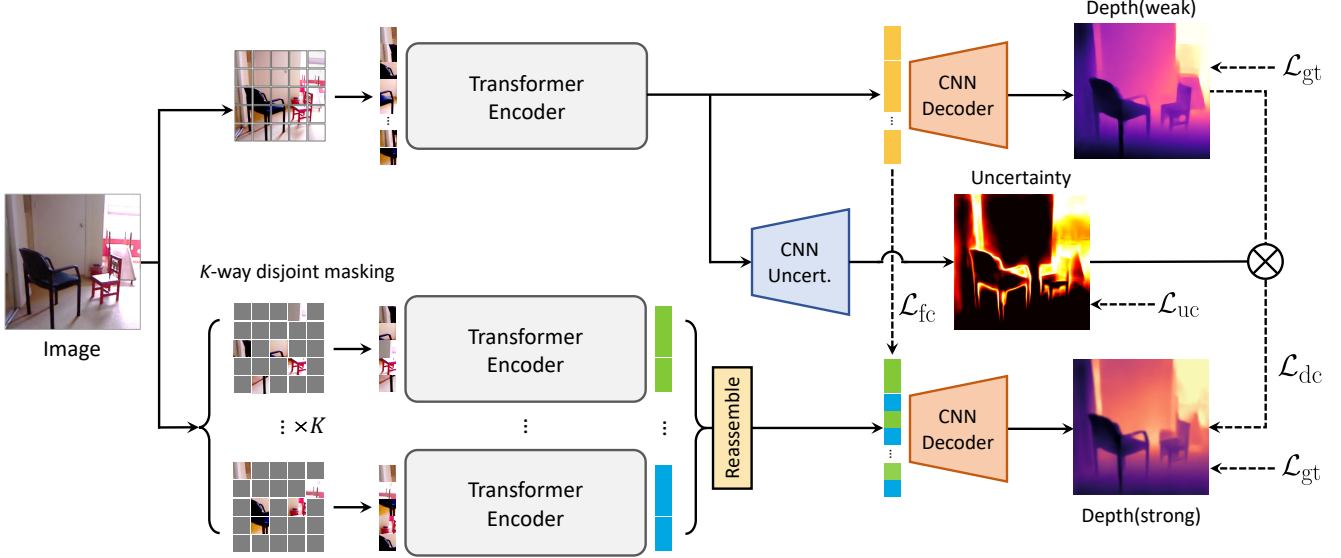


Figure 3. **Overview of MaskingDepth architecture.** It consists of two main components; a branch using full tokens (top), and a branch using  $K$ -way disjoint masked tokens (bottom), where  $K$ -number of subsets are encoded independently and concatenated before decoding. We use consistency loss  $\mathcal{L}_{dc}$  to make predictions between original and augmented images consistent, aided by an uncertainty measure. Feature consistency loss  $\mathcal{L}_{fc}$  is also applied to facilitate the convergence.

one of the most successful methods for pre-training in NLP, related works have explored a variety of masked image prediction strategies suited for Transformers [4, 29]. ViT [13] studied a masked patch prediction to facilitate representation learning, and BEiT [4] extended upon this by predicting discrete tokens. Recent literature [66, 29] introduce an extremely simple yet effective approach. Masked autoencoder (MAE) [29] utilizes only unmasked tokens to encode meaningful representations. In addition, MRA [67] leverages this strategy to generate augmented images. In this paper, we propose an effective data augmentation strategy that takes advantage of masked image modeling.

### 3. Methodology

#### 3.1. Problem Formulation

Let us denote a color image and its corresponding depth map as  $I$  and  $D$ , respectively. The objective of monocular depth estimation is to learn a mapping function  $f$  from the image  $I$  to its corresponding depth  $D$  such that  $D = f(I)$ . Recent learning-based methods formulate the mapping function with convolutions [16, 61, 34] or Transformers [51, 68, 43] as a neural network  $f_\theta$  with parameters  $\theta$ . To train the monocular depth estimation networks  $f_\theta$  in a supervised manner, the ground-truth  $D_{gt}$  is required, but building large-scale dense depth data is notoriously challenging [19, 65]. In addition, to alleviate depth capture errors, post-processing [59, 20, 54] is essential, which introduces further burden.

In this paper, we present a novel semi-supervised learning framework that facilitates the model to learn monocular

depth estimation on a large number of unlabeled data with sparse depth annotations. As shown in Fig. 2, for the first time we introduce consistency regularization between two differently augmented views from the same image to train the monocular depth estimation network.

#### 3.2. Overview

Given an image  $I$ , we build two different branches, one for processing an image passed through weak augmentation (called weak branch) and the other for a strongly augmented image (called strong branch), where the consistency between the two images through the networks  $f_\theta$  is encouraged. In particular, a weakly-augmented image  $I_{weak}$  and a strongly-augmented image  $I_{strong}$  are fed to the network  $f_\theta$ , and then consistency is defined as follows:

$$\mathcal{L} = \mathcal{D}(\text{sg}(f_\theta(I_{weak})), f_\theta(I_{strong})), \quad (1)$$

where  $\text{sg}(\cdot)$  is a stop-gradient operation and  $\mathcal{D}(\cdot, \cdot)$  is a distance function, e.g., mean squared error (MSE) [62] or KL-divergence [35]. In this setting, we can interpret  $f_\theta(I_{weak})$  as a pseudo ground-truth or pseudo-label. To effectively implement this strategy, appropriate data augmentation techniques are important.

However, it is challenging to make difference between two branches in monocular depth estimation since depth-specific data augmentation techniques have been rarely studied [31, 33]. Furthermore, conventional data augmentation techniques such as crop [11] and rotation [22], which have been successfully used in classification tasks, are no longer effective for monocular depth estimation as they can lead to geometric inconsistency [12].

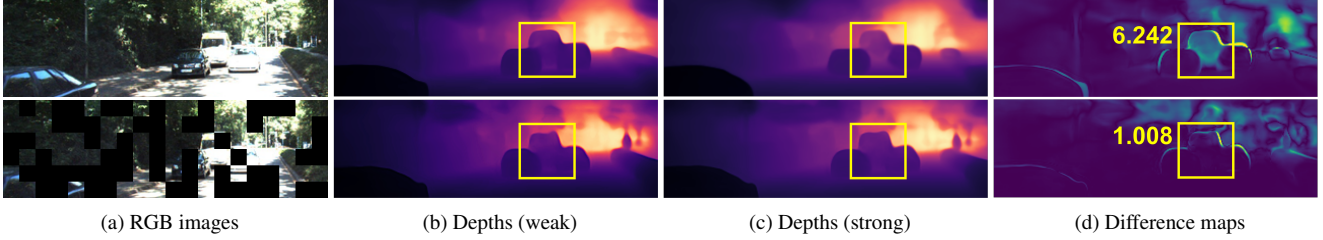


Figure 4. **Effectiveness of our masking strategy to handle scale ambiguity:** (a) RGB image and its masked one. The first row of (b) and (c) are naïve masking results, and the second row of (b) and (c) are our masking results. In (d), we visualize the difference map between (b) and (c). We denote the mean scale difference in the boxed area. Our method better generates scale-consistent results, which in turns helps to better learn the monocular depth estimation networks.

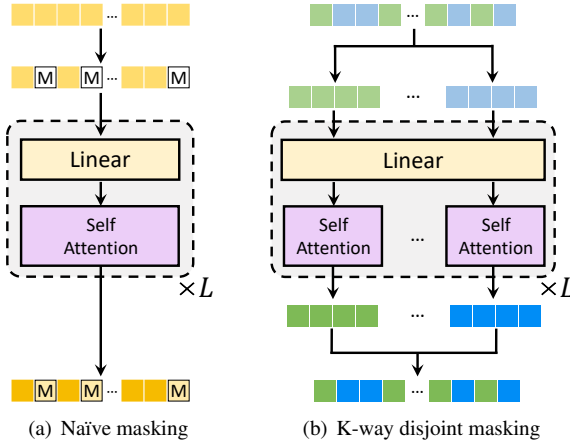


Figure 5. **Illustration of masking:** (a) naïve token masking [66, 4] and (b) our K-way disjoint masking. Compared to conventional masking [66, 4], our masking strategy consistently well produces dense depth maps because it considers the entire set of tokens during decoding.

To address this issue, we present a novel data augmentation technique, inspired by recent masked image modeling techniques [66, 29, 2], which allows for generating geometrically consistent pseudo depth maps while applying sufficient perturbations to the inputs. As illustrated in Fig. 3, our proposed framework follows the backbone model  $f_\theta$  [51] by consisting of a Transformer-based encoder  $f_\theta^{\text{enc}}$ , which takes a tokenized image and outputs encoded features [13], and a CNN-based decoder  $f_\theta^{\text{dec}}$ . In addition, we encourage not only feature similarities [4] but also depth similarities between the two branches processing the two augmented views. To aid the latter, we present uncertainty estimation [32, 50] that helps the convergence of training by filtering out the noise of pseudo labels.

### 3.3. Naïve Masking and Its Limitations

Recent masked image modeling techniques for vision Transformers [4, 66, 29] are effective as data augmentation, and MRA [67] show promising potential. The most naïve way to formulate masked image modeling as augmentation is to simply mask out the tokens. Specifically, given an im-

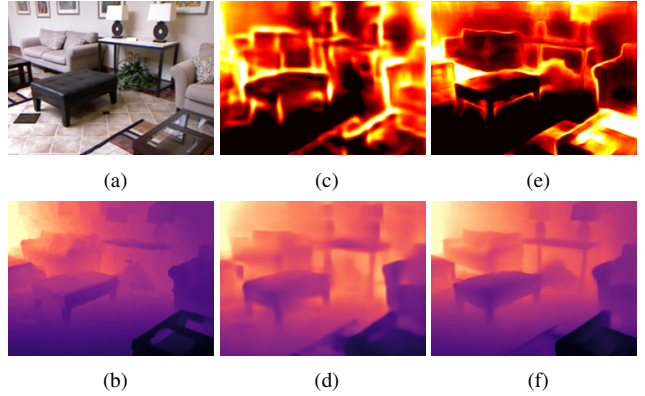


Figure 6. **Examples of estimated depths and uncertainty maps:** (a) RGB, (b) ground-truth depth map, predicted depth maps and their corresponding uncertainty maps by the networks trained with (c), (d) 100 and (e), (f) 10,000 labeled frames and 40K unlabeled frames.

age  $I \in \mathbb{R}^{h \times w \times 3}$ , we reshape it into a sequence of flattened non-overlapped 2D patches  $X \in \mathbb{R}^{N \times P}$ , where  $h \times w$  is the resolution of the original image,  $P = p \times p \times 3$  and  $p \times p$  is the resolution of each image patch, and  $N = hw/p^2$ . These flattened 2D patches  $X$  are embedded by a trainable linear projection [13] operator, which proceeds to be fed into the Transformer encoder  $f_\theta^{\text{enc}}$ . By applying the randomly sampled mask, the sequence of flattened 2D patches  $X$  can be transformed into  $X'$ . Note that similar techniques were also used to increase the robustness of Transformers for image-level or pixel-level classification such as segmentation [66, 29].

Meanwhile, monocular depth estimation heavily depends on contextual information when constructing depth maps. However, naïve masking does not capture the overall context, impeding the ability to generate reliable depth predictions. As shown in Fig. 4, applying a naïve masking strategy to monocular depth estimation causes scale ambiguity issue between results from weakly- and strongly-augmented branches during filling the missing regions, and the risk of missing out small-scale objects.



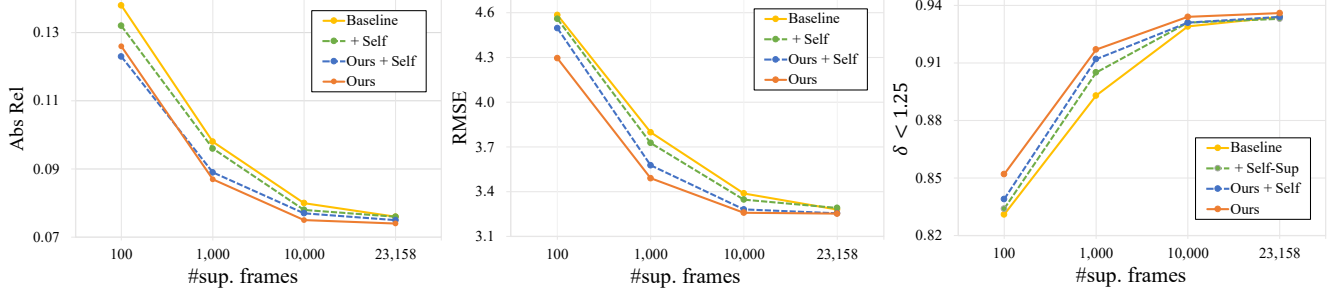


Figure 7. **Quantitative results on the KITTI dataset in a sparsely-supervised setting.** ‘Baseline’ only uses a sparse depth, and ‘Self’ indicates existing self-supervised strategies [19, 24]. ‘Ours’ indicates the proposed semi-supervised framework.

### 3.4. $K$ -way Disjoint Masking

To address this, we present a  $K$ -way disjoint masking technique, where a  $K$ -disjoint set of tokens are encoded independently, then concatenated and decoded simultaneously, as illustrated in Fig. 5. By capturing the entire scene from the partially divided inputs, our method can reduce inherent ambiguity [48] and lead to coherent results, as shown in Fig. 4. Moreover, since it enforces scale consistency by keeping the image size and orientation unaltered, the  $K$ -disjoint masking strategy can also act as data augmentation. Specifically, we divide the sequence of flattened 2D patches  $X \in \mathbb{R}^{N \times P}$  into  $K$  non-overlapping subsets  $X_k$  for  $k \in \{1, \dots, K\}$ , with  $X_k \in \mathbb{R}^{M \times P}$ , where  $M$  is set to be a random value smaller than  $N$  to avoid learning with a fixed size of the tokens set. In other words, the concatenation of all the  $X_k$  tokens should reconstruct the original token representation  $X$ , while maintaining the proper position ordering such that

$$X = [X_1, X_2, \dots, X_K], \quad (2)$$

where  $[\cdot]$  denotes a concatenation operator. By independently encoding  $X_k$  to the latent vector  $\mathbf{z}_k$  such that  $\mathbf{z}_k = f_{\theta}^{\text{enc}}(X_k)$ , unlike original Transformer-based encoding, i.e.,  $\mathbf{z} = f_{\theta}^{\text{enc}}(X)$ , the limited candidates are considered when running self-attention computation, which in turn implements an augmentation over tokens.

Then, to decode all the  $\mathbf{z}_k$ , we reassemble them as  $\bar{\mathbf{z}} = [\mathbf{z}_1, \mathbf{z}_2, \dots, \mathbf{z}_K]$  and obtain the final depth  $D = f_{\theta}^{\text{dec}}(\bar{\mathbf{z}})$ .

In our framework, we control the intensity of augmentations to the networks by adjusting  $K$ . In our experiments, we empirically set  $K = 1$  for the weak branch, and  $K = 64$  for the strong branch, which generate decoded depth maps  $D_{\text{weak}}$  and  $D_{\text{strong}}$ , respectively.

### 3.5. Loss Functions

To train the networks we adopt a sparse supervised loss and the proposed unsupervised loss. In addition, we adopt a loss for modeling the uncertainty of the pseudo ground-truth produced by the weak branch and a feature consistency loss.  $\|\cdot\|_1$  and  $\|\cdot\|_2$  are  $\ell_1$  and  $\ell_2$  loss functions, respectively.

**Sparse supervised loss.** When sparsely depth-labeled data is available to train the network, we can minimize the supervised loss function  $\mathcal{L}_{\text{gt}}$  between the predicted  $D$  and sparse ground-truth  $D_{\text{gt}}$  such that

$$\mathcal{L}_{\text{gt}} = \|D - D_{\text{gt}}\|_1. \quad (3)$$

A small number of fully annotated data used in a supervised manner across both branches allows the network model to ignite the learning process, which is then carried out mainly on unlabeled data through consistency regularization.

**Depth consistency loss.** Our loss function encourages depth prediction of the strongly-augmented image to be close to the prediction of the weakly-augmented image, enabling pixel-level learning without the need for annotated ground-truths, thus it serving as an effective solution to data hunger caused by sparse annotations. The depth consistency loss  $\mathcal{L}_{\text{dc}}$  assisted by the uncertainty map  $U(D_{\text{weak}})$  can be written as:

$$\mathcal{L}_{\text{dc}} = \text{sg}(U(D_{\text{weak}})) \odot \|\text{sg}(D_{\text{weak}}) - D_{\text{strong}}\|_1. \quad (4)$$

where  $\odot$  denotes hadamard product.

**Uncertainty loss.** To filter out the noise on pseudo labels, we train the uncertainty module. This module, which is a key ingredient in our framework, allows for transferring only reliable depth knowledge from weak branch to strongly augmented branch. To model such uncertainty, we leverage a negative log-likelihood minimization [32] as:

$$\mathcal{L}_{\text{uc}} = \frac{\|D - D_{\text{gt}}\|_1}{U(D)} + \log(U(D)), \quad (5)$$

where  $U(D)$  denotes the uncertainty map related to the predicted depth map  $D$ . By training the network to model its uncertainty, predictions on unlabeled data will be trusted if highly confident, as shown in Fig. 6.

**Feature consistency loss.** Within our framework, geometric distortions are not applied to the two branches, thus

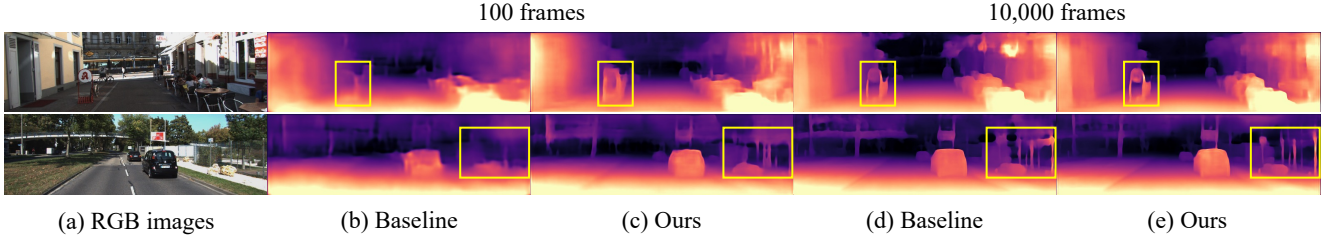


Figure 8. **Qualitative results on the KITTI dataset [20]:** (a) RGB images, predicted depth maps by (b), (d) baseline, and (c), (e) ours using 100 and 10,000 labeled frames, respectively.

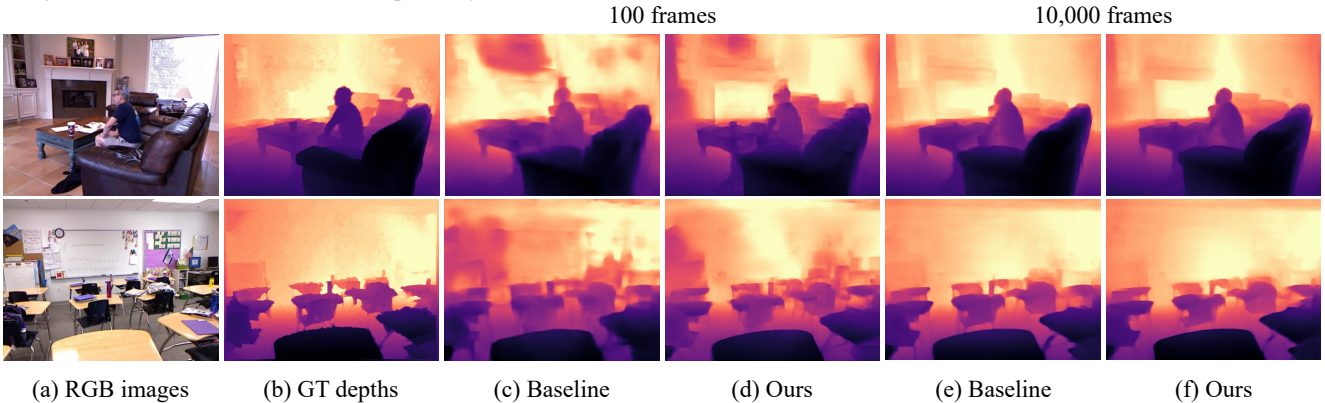


Figure 9. **Qualitative results on the NYU-Depth-v2 dataset [54]:** (a) RGB images, (b) ground-truth depth maps, and predicted depth maps by (c), (e) baseline, and (d), (f) ours using 100 and 10,000 labeled frames, respectively.

the encoded feature consistency can also be encouraged. The feature consistency loss is then defined as

$$\mathcal{L}_{fc} = \|\mathbf{z}_{\text{weak}} - h(\mathbf{z}_{\text{strong}})\|_2, \quad (6)$$

where  $h(\cdot)$  is the additional MLP predictor head, which provides better results as shown in the literature [5, 25] and prevents collapse [71].

**Total loss.** By considering all the loss terms, the final loss is defined as  $\mathcal{L} = \mathcal{L}_{gt} + \lambda_{dc}\mathcal{L}_{dc} + \lambda_{uc}\mathcal{L}_{uc} + \lambda_{fc}\mathcal{L}_{fc}$ , where  $\lambda_{uc}$ ,  $\lambda_{dc}$ , and  $\lambda_{fc}$  represent hyper-parameters.

## 4. Experiments

### 4.1. Implementation Details

We implemented our MaskingDepth with the Pytorch library [47]. We conduct all our experiments on 24GB RTX-3090 GPUs, using DPT-Base [51] as a backbone model. We set the learning rate to  $10^{-5}$  for the encoder and  $10^{-4}$  for the decoder. The encoder is initialized with ImageNet-pretrained [9] weights, whereas the decoder is initialized randomly. We train the entire model with batch size 8 and use Adam optimizer with  $\beta_1 = 0.9$  and  $\beta_2 = 0.999$ .

To avoid collapsing, we balance the ratio of labeled and unlabeled data in one batch to 1:7 similarly to [55]. Besides our new data augmentation approach, we adopt flipping and jittering, widely used in the literature [14, 21]. For confidence estimation, we train the network to predict the log variance because it is more numerically stable [32] than

regressing the variance itself, as the loss avoids any division by zero. We use an identical hyperparameter set (i.e.,  $\lambda_{uc} = 1$ ,  $\lambda_{dc} = 1$ ,  $\lambda_{fc} = 1$ ,  $K = 64$  for strong augmentation) for all experiments unless otherwise specified.

### 4.2. Experimental Settings

**Dataset.** We first evaluate the performance of MaskingDepth and others on the KITTI dataset [20] and NYU-Depth-v2 [54]. The KITTI dataset [20] provides outdoor scenes captured by 3D laser data. The RGB images are resized to  $640 \times 192$  resolutions for training. We follow the standard Eigen training/testing split [16]. We use randomly sampled 10,000, 1,000, and 100 images from  $24K$  (i.e., left frames in the Eigen training split) for labeled images during training. We evaluate our trained model on 652 annotated test images for single-view depth estimation, using the improved ground truth by [59]. The NYU-Depth-v2 dataset [54] is composed of various indoor scenes and corresponding depth maps at a resolution of  $640 \times 480$ . We train our network on the same number of labeled images as KITTI, randomly sampled from the original  $40K$  total. The remaining images in the training set are used as unlabeled images. We test our trained model on 654 test images.

**Evaluation metrics.** In our experiments, we follow the standard evaluation protocol of the prior work [16] to evaluate the effectiveness of MaskingDepth. The error metrics are defined as Absolute Relative error (AbsRel), Squared Relative error (SqRel), Root Mean Squared Error (RMSE),

Methods	Sup.	Self.(M)	Self.(S)	Self.	DB.	AbsRel↓	SqRel↓	RMSE↓	RMSElog↓	$\delta\uparrow$
DORN [17]	✓	-	-	-	K	0.072	0.307	2.727	0.120	0.932
Yin et al. [69]	✓	-	-	-	K	0.072	-	3.258	0.117	0.938
DPT-Hybrid [51]	✓	-	-	-	K+Mix	<b>0.062</b>	<b>0.222</b>	<b>2.575</b>	<b>0.092</b>	<b>0.959</b>
DPT-Base [51]*	✓	-	-	-	K	0.074	0.361	3.275	0.117	0.935
Monodepth2 [24]	-	✓	✓	-	K	0.080	0.466	3.681	0.127	0.926
PackNet-SfM [26]	-	✓	-	-	K	0.078	0.420	3.485	0.121	0.931
ManyDepth [64]	-	✓	-	-	K	<b>0.070</b>	<b>0.399</b>	<b>3.455</b>	<b>0.113</b>	<b>0.941</b>
SVSM FT [45]	✓	-	✓	-	K+F	0.077	0.392	3.569	0.127	0.919
Kuznetsov et al. [38]	✓	-	✓	-	K	0.089	0.478	3.610	0.138	0.906
Baek et al. [3]	✓	✓	✓	-	K	0.078	0.381	3.404	0.121	0.930
Guizilini et al. [27]	✓	✓	-	-	K	0.072	0.340	3.265	0.116	0.934
SemiDepth [1]	✓	-	✓	-	K+C	0.078	0.417	3.464	0.126	0.923
<b>MaskingDepth (DPT-Base)</b>	✓	-	-	✓	K+C	<b>0.071</b>	<b>0.316</b>	<b>3.049</b>	<b>0.111</b>	<b>0.941</b>

Table 1. **Quantitative results on the Eigen split of the KITTI dataset [20].** ‘Sup.’, ‘Self.(M)’, and ‘Self.(S)’ indicate supervised, existing self-supervised strategies on video and stereo pairs, respectively. ‘Self.’ denotes our proposed consistency regularization, which needs **no stereo images or video sequences**. ‘K’, ‘C’, and ‘F’ indicate KITTI [20], Cityscapes [8], and FlyingThings3D [45], respectively. ‘Mix’ indicates the dataset proposed from [51], containing 1.4M images, which is approximately 60 times larger than KITTI. ‘\*’ denotes our re-implementation of the model trained on the full dataset.

Methods	DB.	AbsRel↓	RMSE↓	$\delta\uparrow$
DORN [17]	N	0.115	0.509	0.828
BTS [40]	N	0.110	0.392	0.885
DPT-Hybrid [51]	N+Mix	0.110	<b>0.357</b>	<b>0.904</b>
DPT-Base* [51]	N	0.106	0.380	0.899
<b>MaskingDepth (DPT-Base)</b>	N+S	<b>0.104</b>	0.372	<b>0.904</b>

Table 2. **Quantitative results on the NYU-Depth-v2 [54].** ‘N’ and ‘S’ indicate NYU-Depth-v2 and SUN RGB-D [56] datasets, respectively.

Root Mean Squared log Error (RMSElog), and accuracy under the threshold ( $< 1.25$ ) ( $\delta$ ).

### 4.3. Depth Estimation Results

In this section, we investigate the effects of sparse labels on supervised depth training, and how MaskingDepth is able to mitigate the degradation of depth maps when the number of labels is significantly limited. Especially, our method is useful for improving performance by utilizing vast unlabeled data in place of expensive ground-truth depth annotations.

**Robustness of MaskingDepth.** As a baseline, we compare DPT-Base [51] trained on supervised and conventional semi-supervised manners obtained with self-supervised losses [19, 24]. Results for the KITTI dataset [20] using different numbers of supervised frames are shown in Fig. 7. MaskingDepth outperforms the baseline with any arbitrary number of data frames. As the amount is further decreased, the performance of all approaches, except for ours, shows a significant and rapid decline. This is mostly due to the model’s inability to learn the appropriate scale and structure of a scene with such sparse information. However,

Method	Sup			Semi-Sup		
	AbsRel ↓	RMSE ↓	$\delta\uparrow$	AbsRel ↓	RMSE ↓	$\delta\uparrow$
Baseline	0.078	3.370	0.930	-	-	-
CutOut [11]	0.076	3.302	0.932	0.075	3.351	0.931
SimMiM [66]	0.077	3.338	0.931	0.076	3.363	0.931
MAE [29]	<b>0.075</b>	3.291	0.933	<b>0.074</b>	3.280	0.934
<b>MaskingDepth</b>	0.076	<b>3.289</b>	<b>0.934</b>	0.075	<b>3.239</b>	<b>0.937</b>

Table 3. **Impact of data augmentation.**

as the labels become sparser, the performance degradation of our proposed method progresses more slowly compared to the baseline or naive semi-supervised approach using self-supervised losses, and the performance gap gets larger. Note that when MaskingDepth is incorporated with the existing self-supervised approach, the performance gain was marginal because the existing solution cannot avoid increasing inherent scale ambiguity from the self-supervised loss function. We also provide a qualitative comparison of the baseline and our method on the KITTI dataset in Fig. 8 and the NYU-Depth-v2 dataset in Fig. 9.

**Comparison to other methods.** As our method does not rely on stereo or video sequence frames, it is agnostic to the configuration of the unlabeled training set. Table 1 compares our semi-supervised method that uses additional data against existing approaches. We trained our model on the KITTI dataset [20] as labeled data and the additional Cityscape dataset [8] as additional unlabeled data. In the results, our method achieves significant improvement in comparison to the baseline by utilizing unlabeled data and surpasses the state-of-the-art in semi-supervised depth estimation methods. Moreover, despite using a smaller model capacity and a fewer annotated data, MaskingDepth shows competitive performance against DPT-Hybrid. A similar

Methods	D	U	F	AbsRel↓	RMSE↓	$\delta\uparrow$
Baseline	-	-	-	0.136	4.585	0.833
MaskingDepth	✓	-	-	0.132	4.355	0.848
	✓	✓	-	0.126	4.296	0.851
	-	-	✓	0.131	4.422	0.849
	✓	✓	✓	<b>0.124</b>	<b>4.263</b>	<b>0.855</b>

Table 4. **Ablation study on main components:** Depth consistency (D), Uncertainty (U), and Feature consistency (F).

Methods	Cap	AbsRel↓	SqRel↓	RMSE↓	RMSElog↓	$\delta\uparrow$
Kundu <i>et al.</i> [37]	50m	0.203	1.734	6.251	0.284	0.687
T2Net [73]	50m	0.168	1.199	4.674	0.243	0.772
GASDA [72]	50m	0.143	0.756	3.846	0.217	0.836
SharinGAN [49]	50m	<b>0.109</b>	<b>0.673</b>	3.770	0.190	<b>0.864</b>
<b>MaskingDepth</b>	50m	0.129	0.719	<b>3.475</b>	<b>0.180</b>	0.845
GASDA [72]	80m	0.149	1.003	4.995	0.227	0.824
SharinGAN [49]	80m	<b>0.116</b>	<b>0.939</b>	5.068	0.203	<b>0.850</b>
<b>MaskingDepth</b>	80m	0.136	1.020	<b>4.726</b>	<b>0.190</b>	0.833

Table 5. **Domain adaptation on the KITTI dataset [20].** For the training data, KITTI dataset [20] and vKITTI dataset [18] were used.

trend can be seen in Table 2, where our method utilizes the SUN RGB-D [56] dataset as additional unlabeled data and NYU-Depth-v2 as labeled data.

#### 4.4. Ablation Study

We analyze the effectiveness of different design choices in our framework on the KITTI dataset [20]. We exploit 10,000 and 100 randomly sampled images, respectively for data augmentation and other ablation studies.

**Data augmentation.** We evaluate our proposed  $K$ -way disjoint masking as augmentation and compare it to different MIM methods, including SimMIM [66] and MAE [29], and another data augmentation method, CutOut [11]. We evaluate these methods in both fully supervised and semi-supervised settings using a baseline model, which is trained in a supervised manner and without any augmentation. The results are summarized in Table 3. Although other augmentation methods improved the model performance, they also increased the inherent ambiguity. Our augmentation not only reduces the inherent ambiguity but also achieves the best performance by capturing the entire scene.

**Loss functions.** We examine each component of the loss function in our method. It consists of four components: the sparse supervised term, the depth consistency term, the feature consistency term, and the uncertainty term. To evaluate the impact of each component, we start by using only the sparse supervised loss as a baseline and then study the effect of adding each of the other three components. As shown in Table 4, the performance of our network improves as each component of the loss function is added. We can



Figure 10. **Qualitative results of KITTI [20] data samples for models trained with vKITTI datasets [18]:** (a) RGB, (b) predicted depth maps, MaskingDepth proves to work well in domain adaptation task on real-world images.

see that using all components together leads to a significant improvement.

**The number of  $K$ .** To study the influence of the masking ratio, we train the network by adopting different values of  $K$  for the strong branch, respectively  $K = 4, 16, 64$ , and 128. The quantitative evaluation results for this study is shown in Supplementary materials. Starting from  $K = 4$ , the error decreases with the increase of  $K$ , until degrading for  $K = 128$ . We set  $K = 64$  as the default since it yields the best results.

#### 4.5. Domain Adaptation

Inspired by [46], we simply apply MaskingDepth to the task of unsupervised domain adaptation using virtual KITTI (vKITTI) [18] and KITTI [20] as synthetic and real datasets, respectively. As demonstrated in Table 5, MaskingDepth achieves reasonable performance compared to others. While other methods rely on generative models which are large and hard to train, our method is lightweight and easily adaptable without an external network. Fig. 10 shows some well-adapted results in the real-world domain.

### 5. Conclusion

In this paper, we presented MaskingDepth, a novel semi-supervised framework for monocular depth estimation using consistency regularization. MaskingDepth allows leveraging unlabeled data without requiring either stereo or sequential frames. To this end, we also proposed a data augmentation method, called  $K$ -way disjoint masking. We have shown that  $K$ -way disjoint masking makes consistency regularization framework more stable by utilizing an uncertainty network. Our proposed method showed significant improvement on extremely sparse labeled data and superior results compared to other semi-supervised approaches. For future work, we plan to extend our method to other dense prediction tasks.

**Acknowledgements.** This research was supported in part by Autonomous Driving Center, R&D Division, Hyundai Motor Company.



# Appendix

In this appendix, we provide more results on experiments and more implementation details of our framework.

## Appendix A. Quantitative Details

More detailed quantitative results of our proposed method and conventional self-supervised method on the KITTI dataset [20] are shown in Table 6. Moreover, to verify the generalization ability of our framework, we evaluated our framework on the NYU-Depth-v2 dataset [54]. Results are shown in Table 7.

Methods	# sup. frames	AbsRel ↓	SqRel ↓	RMSE ↓	RMSElog ↓	$\delta\uparrow$
Baseline	23,158	$0.076 \pm 0.003$	$0.365 \pm 0.004$	$3.290 \pm 0.015$	$0.118 \pm 0.001$	$0.934 \pm 0.001$
	10,000	$0.079 \pm 0.001$	$0.379 \pm 0.007$	$3.388 \pm 0.019$	$0.121 \pm 0.009$	$0.929 \pm 0.001$
	1,000	$0.098 \pm 0.004$	$0.515 \pm 0.030$	$3.785 \pm 0.013$	$0.142 \pm 0.005$	$0.899 \pm 0.005$
	100	$0.135 \pm 0.005$	$0.728 \pm 0.019$	$4.585 \pm 0.048$	$0.186 \pm 0.011$	$0.831 \pm 0.005$
	10	$0.201 \pm 0.023$	$1.508 \pm 0.045$	$6.163 \pm 0.082$	$0.268 \pm 0.029$	$0.701 \pm 0.021$
Baseline + Self. (M)	23,158	$0.076 \pm 0.002$	$0.367 \pm 0.007$	$3.291 \pm 0.020$	$0.117 \pm 0.001$	$0.933 \pm 0.002$
	10,000	$0.078 \pm 0.001$	$0.376 \pm 0.006$	$3.347 \pm 0.043$	$0.119 \pm 0.002$	$0.931 \pm 0.001$
	1,000	$0.096 \pm 0.002$	$0.523 \pm 0.024$	$3.750 \pm 0.033$	$0.140 \pm 0.002$	$0.900 \pm 0.004$
	100	$0.132 \pm 0.004$	$0.759 \pm 0.014$	$4.559 \pm 0.044$	$0.184 \pm 0.003$	$0.834 \pm 0.004$
	10	$0.210 \pm 0.020$	$1.322 \pm 0.042$	<b><math>5.627 \pm 0.080</math></b>	$0.265 \pm 0.027$	$0.711 \pm 0.016$
MaskingDepth + Self. (M)	23,158	$0.079 \pm 0.001$	$0.379 \pm 0.007$	$3.388 \pm 0.019$	$0.121 \pm 0.009$	$0.929 \pm 0.001$
	10,000	$0.076 \pm 0.017$	$0.369 \pm 0.004$	$3.311 \pm 0.011$	$0.117 \pm 0.001$	<b><math>0.935 \pm 0.002</math></b>
	1000	<b><math>0.085 \pm 0.017</math></b>	$0.430 \pm 0.011$	$3.521 \pm 0.012$	$0.129 \pm 0.012$	<b><math>0.918 \pm 0.010</math></b>
	100	<b><math>0.123 \pm 0.003</math></b>	$0.747 \pm 0.018$	$4.497 \pm 0.042$	$0.181 \pm 0.005$	$0.839 \pm 0.005$
	10	<b><math>0.184 \pm 0.011</math></b>	<b><math>1.265 \pm 0.064</math></b>	$5.747 \pm 0.080$	<b><math>0.243 \pm 0.007</math></b>	$0.727 \pm 0.018$
MaskingDepth	23,158	<b><math>0.074 \pm 0.001</math></b>	<b><math>0.362 \pm 0.001</math></b>	<b><math>3.253 \pm 0.012</math></b>	<b><math>0.116 \pm 0.001</math></b>	<b><math>0.935 \pm 0.001</math></b>
	10,000	<b><math>0.075 \pm 0.002</math></b>	<b><math>0.362 \pm 0.006</math></b>	<b><math>3.259 \pm 0.020</math></b>	<b><math>0.116 \pm 0.001</math></b>	$0.934 \pm 0.003$
	1,000	$0.088 \pm 0.003$	<b><math>0.419 \pm 0.007</math></b>	<b><math>3.490 \pm 0.020</math></b>	<b><math>0.129 \pm 0.003</math></b>	$0.917 \pm 0.002$
	100	$0.128 \pm 0.004$	<b><math>0.707 \pm 0.013</math></b>	<b><math>4.295 \pm 0.037</math></b>	<b><math>0.173 \pm 0.006</math></b>	<b><math>0.849 \pm 0.006</math></b>
	10	$0.197 \pm 0.019$	$1.378 \pm 0.032$	$5.650 \pm 0.091$	$0.261 \pm 0.030$	<b><math>0.723 \pm 0.017</math></b>

Table 6. **Quantitative results** on the KITTI dataset [20] in a sparsely-supervised setting using sparse labels from [59]. For each row, we trained 5 independent models with randomly selected labels from entire dataset to calculate the mean and variance. ‘Self. (M)’ and ‘MaskingDepth’ indicate monocular self-supervised learning and proposed consistency regularization, respectively. The best results are in **bold**.

Methods	# sup. frames	AbsRel ↓	RMSE ↓	log <sub>10</sub> ↓	δ↑
Baseline	42,602	0.106 ± 0.002	0.380 ± 0.004	<b>0.053 ± 0.001</b>	0.897 ± 0.001
	10,000	0.112 ± 0.004	0.389 ± 0.006	0.057 ± 0.003	0.893 ± 0.003
	1,000	0.141 ± 0.008	0.447 ± 0.009	0.066 ± 0.004	0.843 ± 0.006
	100	0.199 ± 0.011	0.604 ± 0.014	0.086 ± 0.005	0.694 ± 0.011
	10	0.321 ± 0.040	0.872 ± 0.042	0.124 ± 0.008	0.523 ± 0.027
MaskingDepth	42,602	<b>0.105 ± 0.002</b>	<b>0.379 ± 0.003</b>	<b>0.053 ± 0.001</b>	<b>0.899 ± 0.001</b>
	10,000	<b>0.107 ± 0.002</b>	<b>0.386 ± 0.006</b>	<b>0.054 ± 0.002</b>	<b>0.896 ± 0.002</b>
	1,000	<b>0.135 ± 0.007</b>	<b>0.440 ± 0.008</b>	<b>0.065 ± 0.004</b>	<b>0.853 ± 0.005</b>
	100	<b>0.182 ± 0.008</b>	<b>0.594 ± 0.012</b>	<b>0.083 ± 0.003</b>	<b>0.718 ± 0.010</b>
	10	<b>0.292 ± 0.031</b>	<b>0.814 ± 0.037</b>	<b>0.112 ± 0.006</b>	<b>0.561 ± 0.021</b>

Table 7. **Quantitative results** on the NYU-Depth-v2 dataset [54] in a sparsely-supervised setting. For each row, we trained 5 independent models with randomly selected labels from the entire dataset to calculate the mean and variance.

## Appendix B. Additional Results

In the main paper, we have visualized comparisons of the baseline and our methods on the NYU-Depth-v2 dataset [54] and KITTI dataset [20]. In this section, we provide additional qualitative results after having trained on 100 and 10,000 frames in Fig. 11 and Fig. 12. Our method provides better depth results than the baseline.

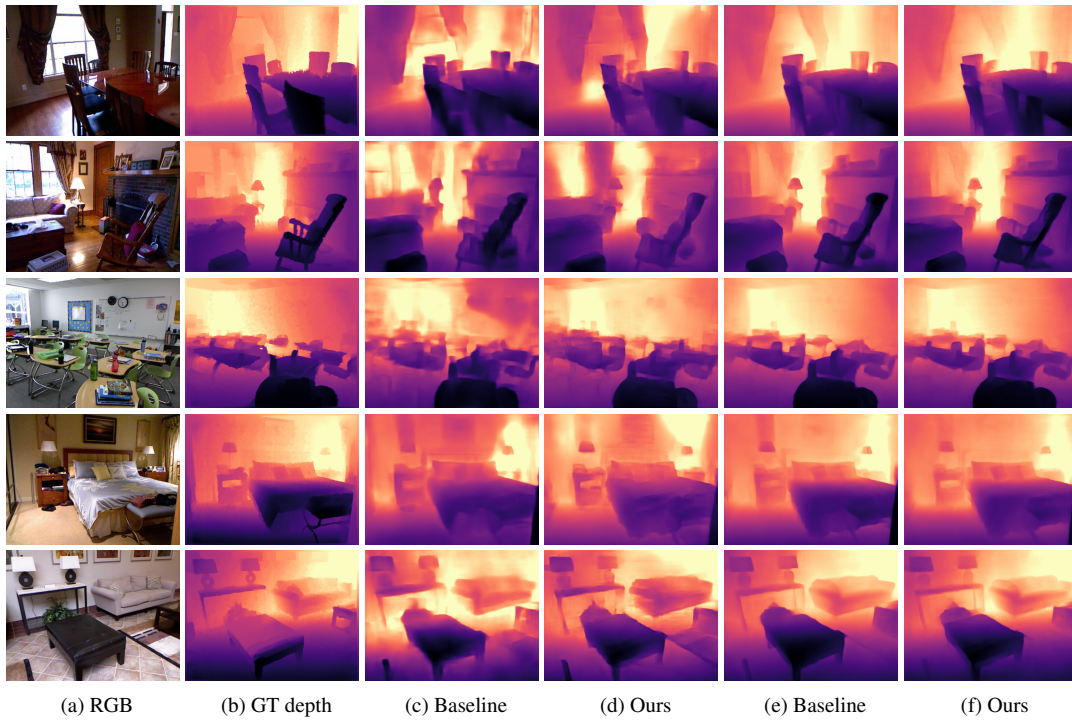


Figure 11. **Qualitative results on the NYU-Depth-v2 dataset [54]:** (a) RGB image, (b) ground-truth depth map, and predicted depth maps by (c), (e) baseline, and (d), (f) ours using 100 and 10,000 labeled frames, respectively.

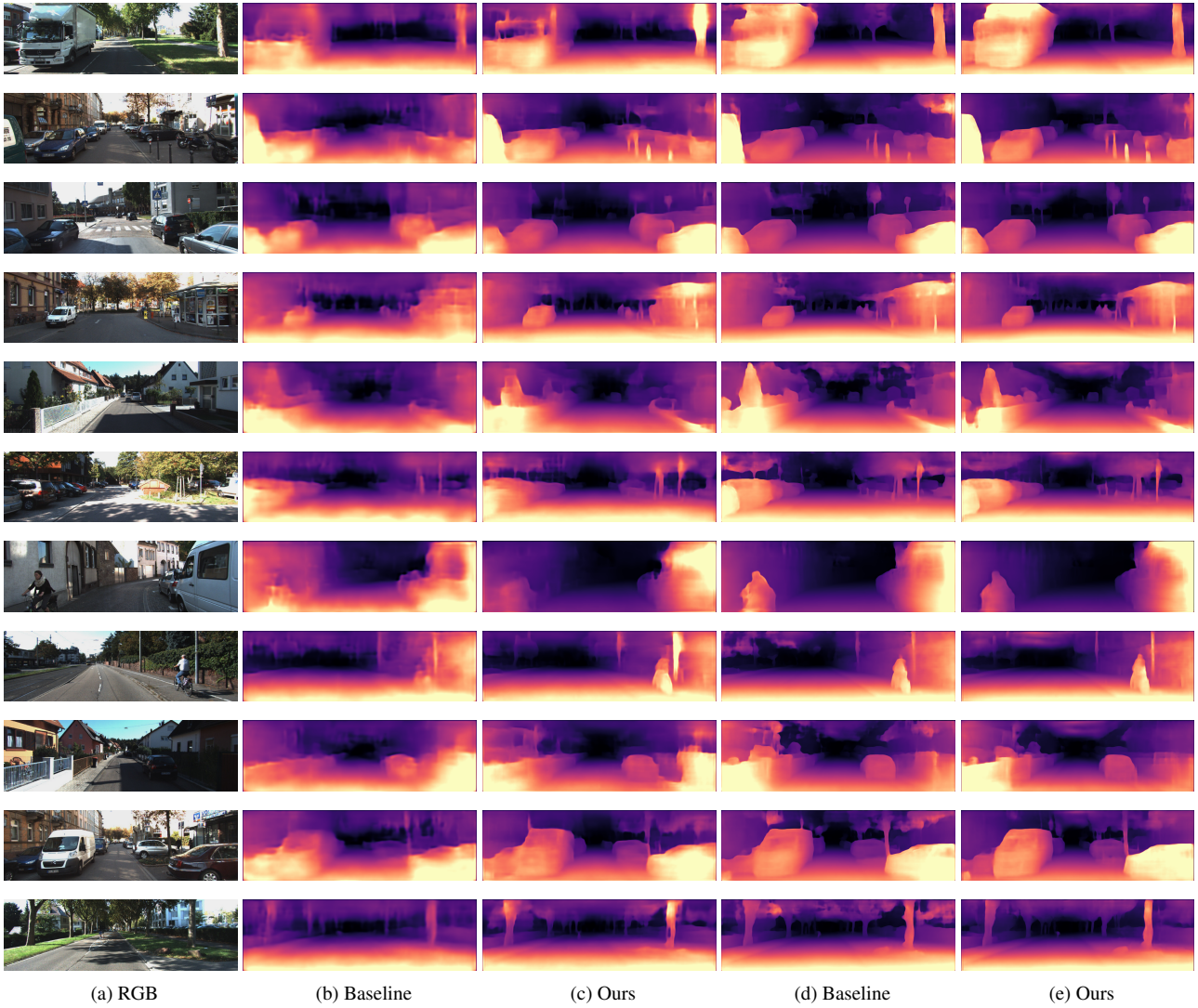


Figure 12. **Qualitative results on the KITTI dataset [20]:** (a) RGB image, predicted depth maps by (b), (d) baseline, and (c), (e) ours using 100 and 10,000 labeled frames, respectively.

## Appendix C. Additional Ablation Study

In the main paper, we control the intensity of the proposed augmentation strategy to the networks by adjusting  $K$ . The quantitative evaluation results for this study are presented in Table 8. To further enhance the representation power of the encoder, we incorporate a feature consistency loss between the encoded features of the weak and strong branches. Our experiments reveal that training did not reach convergence when the predictor head was removed, which led to collapsing. Our framework without a predictor head is conceptually analogous to a vanilla siamese network, which cannot prevent collapsing [71]. In this set of experiments, we evaluate the performance of the predictor head used to provide better results with feature consistency loss. Table 9 displays the results, indicating that a simple MLP is preferred for computational efficiency, despite a single Transformer block or an MLP showing comparable performance.

$K$	AbsRel ↓	RMSE ↓	$\delta\uparrow$
$K = 4$	0.131	4.456	0.850
$K = 16$	0.128	4.298	<b>0.855</b>
$K = 64$	<b>0.124</b>	<b>4.263</b>	<b>0.855</b>
$K = 128$	0.132	4.382	0.849

Table 8. Influence of the number of  $K$ .

Method	Blocks	AbsRel ↓	$\delta\uparrow$
w/o head	-	0.317	0.423
Transformer	1	0.125	<b>0.856</b>
Transformer	2	0.129	0.848
MLP	2	<b>0.124</b>	0.855

Table 9. Comparison of using different predictor head.

## Appendix D. Domain Adaptation

In the main paper, we simply extend MaskingDepth to domain adaptation by following [46] and provide the additional qualitative results in this section. As demonstrated in Fig. 13, unlike generative models, MaskingDepth is simply adaptable and lightweight while achieving reasonable performance in the domain adaptation from virtual KITTI (synthetic) [18] to KITTI (real) [20].



Figure 13. Qualitative results on the KITTI dataset [20]: (a), (c) RGB image, and (b), (d) depth map. Our framework proves to work well in domain adaptation task on real-world images.



## Appendix E. Limitations of Naïve Masking

In this section, we visualize failure cases of naïve masking strategy, specifically “missing object” and “scale ambiguity” cases. As shown in Fig. 14 we found that small objects often disappear even very small parts of them are masked out. In addition, locally inconsistent depth maps are shown in Fig. 15. These cases can cause the performance drop in consistency regularization framework.

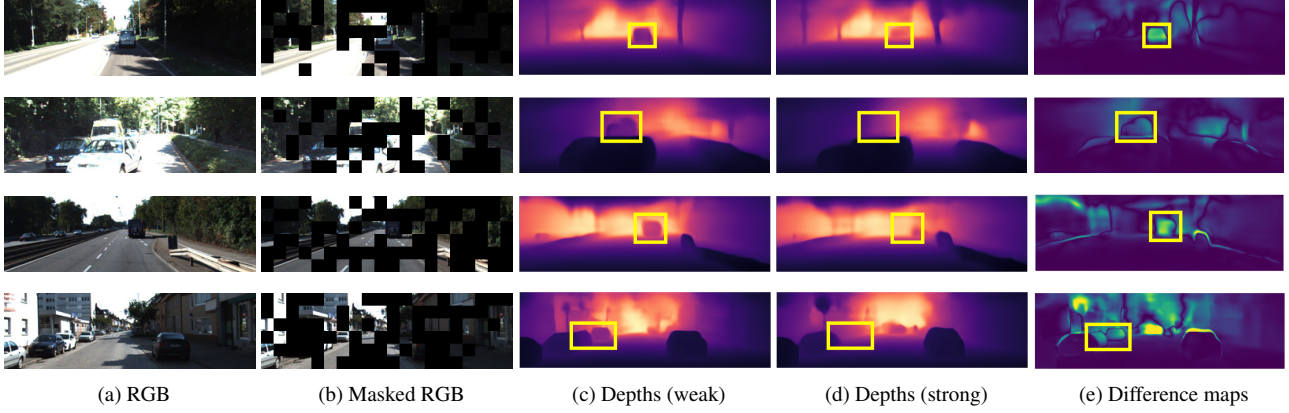


Figure 14. **Missing object cases of naïve masking on the KITTI dataset [20]:** (a) RGB images, (b) masked RGB images, (c) depth maps predicted from (a), (d) depth maps predicted from (b), and (e) difference maps between (c) and (d).

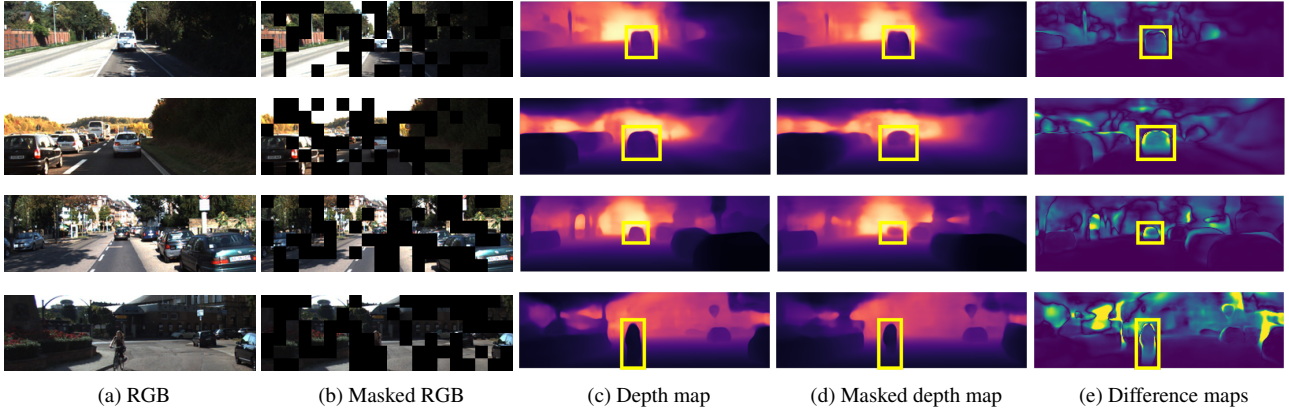


Figure 15. **Scale ambiguity cases of naïve masking on the KITTI dataset [20]:** (a) RGB images, (b) masked RGB images, (c) depth maps predicted from (a), (d) depth maps predicted from (b), and (e) difference maps between (c) and (d).

## Appendix F. More Implementation Details

**PyTorch-like Pseudo-code for  $K$ -way disjoint masking.** We provide pseudo-code for  $K$ -way disjoint masking, in order to show how our novel technique can be implemented independently. This enables the effect of data augmentation while preserving the geometry.

---

**Algorithm 1** Pseudo Code of  $K$ -way disjoint masking

---

```
# Input: Transformer are basic transformer encoder blocks
# Input: X (B x N x P) is patch embeddings
# where N is number of patches and P is embedding dimension
# Input: K is number of masking subsets.
# Output: Z (B x N x P) is K-way disjointly encoded features
def K_way_masked_transformer(transformer, X, K):
    B, N, _ = X.shape
    batch_range = torch.arange(B)[:, None]
    rand_indices = torch.rand(B, N).argsort(dim = -1)
    X = X[batch_range, rand_indices]
    # patch wise random shuffling on X
    # X is no longer spatial order after shuffling

    v = sorted([random.randint(1, N-1) for i in range(int(K-1))] + [0, N])
    # sampling subset split point randomly
    mask_v = torch.zeros(len(v[:-1]), N)
    for i in range(len(v[:-1])):
        mask_v[i, v[i]:v[i+1]] = 1.0

    attention_mask = mask_v.transpose(0,1) @ mask_v
    # mask has shape of (B x N x N)
    # attention matrix masking from different subset
    # by applying this attention mechanism proceeds semi-globally

    Z_ = transformer(x, attention_mask)
    # Z (B x N x P) is K-way masked token embeddings
    reform_indices = torch.argsort(rand_indices, dim=1)

    return Z_[batch_range, reform_indices]
    # reassemble features to spatial order and return

# In the transformer, attention method
# Input: Q, K, V (B x N x P) is Query, Key, Value vectors
# Input: mask (B x N x N) attention mask
# Output: V' (B x N x P) mask attentioned Value vectors
def attention(Q, K, V, mask):
    dots = torch.matmul(Q, K.transpose(-1, -2)) * sqrt(Q.shape[-1])
    ## general attention matrix that has shape of (B x N x N)
    if not(mask == None):
        dots[:, :, mask==0.0] = -10.0
    ## replace value of masked region with negatives befor softmax
    ## so it's attention distribution value goes nearly zero after softmax
    attn = Softmax(dots, dim=-1)
    V = torch.matmul(attn, V)
    return V
```

---

**Network Architecture Details.** We summarize the detailed network architecture of our model in Table 10. Our encoder follows ViT [13] without class token. We use 12 transformer blocks(ViT-Base) and extract features 2, 5, 8, and 11 for skip connection input ( $0 \leq N \leq 11$ ). The Decoder structure follows DPT [51], and the Decoder part in the Table 10 indicates 4 skip connections. However, there are no readout operations because no class token is used.

## Appendix G. Limitations and Broader Impact

**Limitations.** In this paper, we introduce a novel consistency regularization framework for semi-supervised monocular depth estimation, called MaskingDepth. However, our approach learns unlabeled data by following the guidance of a small number of labeled data, so it may fail to predict depth in sparse annotations such as sky regions. Another limitation is that our method performs well on the KITTI dataset [20], while the performance improves relatively less on images with a higher variety of content, e.g., as in the NYU-Depth-v2 dataset [54].

**Broader Impact.** In the future, we aim to apply our method in various data domains, and develop the performance of our framework by leveraging the newly studied data augmentation techniques. Our work is an essential study in order to be completely free from the dependence of the data, and provides the possibility to replace the existing self-supervised monocular depth estimation methods which require specific dataset, such as stereo pairs and video sequences.

PatchEmbedding		
Layer	Parameters (in, out, k, s, p)	Output shape ( $C \times H \times W$ )
Conv	(3, 768, 16, 16, 0)	(768, 12, 40)
Rerange	–	( $HW = 480, C = 768$ )

Transformer Encoder N blocks		
Layer	Parameters (in, out)	Output shape ( $C$ )
LayerNorm	–	(768)
Linear-N-1	(768, 2304)	(2304)
Attention	–	(768)
Linear-N-2	(768, 768)	(768)
LayerNorm	–	(768)
Linear-N-3	(768, 3072)	(3072)
GELU	–	(3072)
Linear-N-4	(3072, 768)	(768)

Decoder		
Layer	Parameters (in, out, k, s, p)	Output shape ( $C \times H \times W$ )
Conv-1(Linear-2-4)	(768, 96, 1, 1, 0)	(96, 12, 40)
ConvTranspose-1	(96, 96, 4, 4, 0)	(96, 48, 160)
Conv-2	(96, 256, 3, 1, 1)	(256, 48, 160)
Conv-3(Linear-5-4)	(768, 192, 1, 1, 0)	(192, 12, 40)
ConvTranspose-2	(192, 192, 2, 2, 0)	(192, 24, 80)
Conv-4	(192, 256, 3, 1, 1)	(256, 24, 80)
Conv-5(Linear-8-4)	(768, 384, 1, 1, 0)	(384, 12, 40)
Conv-6	(384, 256, 3, 1, 1)	(256, 12, 40)
Conv-7(Linear-11-4)	(768, 768, 1, 1, 0)	(768, 12, 40)
Conv-8	(768, 768, 3, 2, 1)	(768, 6, 20)
Conv-9	(768, 256, 3, 1, 1)	(256, 6, 20)

Fusion(x)		
Layer	Parameters (in, out, k, s, p)	Output shape ( $C \times H \times W$ )
ReLU	–	(256, h, w)
Conv-10	(256, 256, 3, 1, 1)	(256, h, w)
ReLU	–	(256, h, w)
Conv-11	(256, 256, 3, 1, 1)	(256, h, w)
ReLU	–	(256, h, w)
Fusion-1(Conv-9)	–	(256, 6, 20)
UpSample	–	(256, 12, 40)
Conv-12	(256, 256, 1, 1, 1)	(256, 12, 40)
Fusion-2(Conv-6)	–	(256, 12, 40)
add-2(Fusion-2, Conv-12)	–	(256, 12, 40)
Fusion-4(add-2)	–	(256, 12, 40)
UpSample	–	(256, 24, 80)
Conv-13	(256, 256, 1, 1, 1)	(256, 24, 80)
Fusion-5(Conv-4)	–	(256, 24, 80)
add-3(Fusion-5, Conv-13)	–	(256, 24, 80)
Fusion-6(add-3)	–	(256, 24, 80)
UpSample	–	(256, 48, 160)
Conv-14	(256, 256, 1, 1, 1)	(256, 48, 160)
Fusion-7(Conv-2)	–	(256, 48, 160)
add-4(Fusion-7, Conv-14)	–	(256, 48, 160)
Fusion(add-4)	–	(256, 48, 160)
UpSample	–	(256, 96, 320)
Conv-15	(256, 256, 1, 1, 1)	(256, 96, 320)
Conv-16	(256, 128, 3, 1, 1)	(128, 96, 320)
UpSample	–	(256, 192, 640)
Conv-17	(128, 32, 3, 1, 1)	(32, 192, 640)
ReLU	–	(32, 192, 640)
Conv-18	(32, 1, 1, 1, 0)	(1, 192, 640)
sigmoid	–	(1, 192, 640)

Table 10. Network architecture of our model.



## References

- [1] Ali Jahani Amiri, Shing Yan Loo, and Hong Zhang. Semi-supervised monocular depth estimation with left-right consistency using deep neural network. In *ROBIO*, pages 602–607, 2019.
- [2] Roman Bachmann, David Mizrahi, Andrei Atanov, and Amir Zamir. Multima: Multi-modal multi-task masked autoencoders. *arXiv*, 2022.
- [3] Jongbeom Baek, Gyeongnyeon Kim, and Seungryong Kim. Semi-supervised learning with mutual distillation for monocular depth estimation. *arXiv*, 2022.
- [4] Hangbo Bao, Li Dong, and Furu Wei. Beit: Bert pre-training of image transformers. *arXiv*, 2021.
- [5] Xinlei Chen and Kaiming He. Exploring simple siamese representation learning. In *CVPR*, pages 15750–15758, 2021.
- [6] Jaehoon Cho, Dongbo Min, Youngjung Kim, and Kwanghoon Sohn. A large rgb-d dataset for semi-supervised monocular depth estimation. *arXiv*, 2019.
- [7] Hyesong Choi, Hunsang Lee, Sunkyung Kim, Sunok Kim, Seungryong Kim, Kwanghoon Sohn, and Dongbo Min. Adaptive confidence thresholding for monocular depth estimation. In *ICCV*, pages 12808–12818, 2021.
- [8] Marius Cordts, Mohamed Omran, Sebastian Ramos, Timo Rehfeld, Markus Enzweiler, Rodrigo Benenson, Uwe Franke, Stefan Roth, and Bernt Schiele. The cityscapes dataset for semantic urban scene understanding. In *CVPR*, pages 3213–3223, 2016.
- [9] Jia Deng, Wei Dong, Richard Socher, Li-Jia Li, Kai Li, and Li Fei-Fei. Imagenet: A large-scale hierarchical image database. In *CVPR*, pages 248–255. Ieee, 2009.
- [10] Jacob Devlin, Ming-Wei Chang, Kenton Lee, and Kristina Toutanova. Bert: Pre-training of deep bidirectional transformers for language understanding. *arXiv*, 2018.
- [11] Terrance DeVries and Graham W Taylor. Improved regularization of convolutional neural networks with cutout. *arXiv*, 2017.
- [12] Tom van Dijk and Guido de Croon. How do neural networks see depth in single images? In *Proceedings of the IEEE/CVF International Conference on Computer Vision*, pages 2183–2191, 2019.
- [13] Alexey Dosovitskiy, Lucas Beyer, Alexander Kolesnikov, Dirk Weissenborn, Xiaohua Zhai, Thomas Unterthiner, Mostafa Dehghani, Matthias Minderer, Georg Heigold, Sylvain Gelly, et al. An image is worth 16x16 words: Transformers for image recognition at scale. *arXiv*, 2020.
- [14] Debidatta Dwibedi, Ishan Misra, and Martial Hebert. Cut, paste and learn: Surprisingly easy synthesis for instance detection. In *ICCV*, pages 1301–1310, 2017.
- [15] David Eigen and Rob Fergus. Predicting depth, surface normals and semantic labels with a common multi-scale convolutional architecture. In *Proceedings of the IEEE international conference on computer vision*, pages 2650–2658, 2015.
- [16] David Eigen, Christian Puhrsch, and Rob Fergus. Depth map prediction from a single image using a multi-scale deep network. *NIPS*, 27, 2014.
- [17] Huan Fu, Mingming Gong, Chaohui Wang, Kayhan Batmanghelich, and Dacheng Tao. Deep ordinal regression network for monocular depth estimation. In *CVPR*, pages 2002–2011, 2018.
- [18] Adrien Gaidon, Qiao Wang, Yohann Cabon, and Eleonora Vig. Virtual worlds as proxy for multi-object tracking analysis. In *Proceedings of the IEEE conference on computer vision and pattern recognition*, pages 4340–4349, 2016.
- [19] Ravi Garg, BG Vijay Kumar, Gustavo Carneiro, and Ian Reid. Unsupervised cnn for single view depth estimation: Geometry to the rescue. In *ECCV*, pages 740–756. Springer, 2016.
- [20] Andreas Geiger, Philip Lenz, and Raquel Urtasun. Are we ready for autonomous driving? the kitti vision benchmark suite. In *CVPR*, pages 3354–3361. IEEE, 2012.
- [21] Golnaz Ghiasi, Yin Cui, Aravind Srinivas, Rui Qian, Tsung-Yi Lin, Ekin D Cubuk, Quoc V Le, and Barret Zoph. Simple copy-paste is a strong data augmentation method for instance segmentation. In *CVPR*, pages 2918–2928, 2021.
- [22] Spyros Gidaris, Praveer Singh, and Nikos Komodakis. Unsupervised representation learning by predicting image rotations. *arXiv*, 2018.
- [23] Clément Godard, Oisín Mac Aodha, and Gabriel J Brostow. Unsupervised monocular depth estimation with left-right consistency. In *CVPR*, pages 270–279, 2017.
- [24] Clément Godard, Oisín Mac Aodha, Michael Firman, and Gabriel J Brostow. Digging into self-supervised monocular depth estimation. In *ICCV*, pages 3828–3838, 2019.
- [25] Jean-Bastien Grill, Florian Strub, Florent Altché, Corentin Tallec, Pierre Richemond, Elena Buchatskaya, Carl Doersch, Bernardo Avila Pires, Zhaohan Guo, Mohammad Gheshlaghi Azar, et al. Bootstrap your own latent—a new approach to self-supervised learning. *NIPS*, 33:21271–21284, 2020.
- [26] Vitor Guizilini, Rares Ambrus, Sudeep Pillai, Allan Raventos, and Adrien Gaidon. 3d packing for self-supervised monocular depth estimation. In *CVPR*, pages 2485–2494, 2020.
- [27] Vitor Guizilini, Jie Li, Rares Ambrus, Sudeep Pillai, and Adrien Gaidon. Robust semi-supervised monocular depth estimation with reprojected distances. In *Conference on robot learning*, pages 503–512. PMLR, 2020.
- [28] Xiaoyang Guo, Hongsheng Li, Shuai Yi, Jimmy Ren, and Xiaogang Wang. Learning monocular depth by distilling cross-domain stereo networks. In *ECCV*, pages 484–500, 2018.
- [29] Kaiming He, Xinlei Chen, Saining Xie, Yanghao Li, Piotr Dollár, and Ross Girshick. Masked autoencoders are scalable vision learners. *arXiv*, 2021.
- [30] Jingwei Huang, Zhili Chen, Duygu Ceylan, and Hailin Jin. 6-dof vr videos with a single 360-camera. In *VR*, pages 37–44. IEEE, 2017.
- [31] Yasunori Ishii and Takayoshi Yamashita. Cutdepth: Edge-aware data augmentation in depth estimation. *arXiv*, 2021.
- [32] Alex Kendall and Yarin Gal. What uncertainties do we need in bayesian deep learning for computer vision? *NIPS*, 30, 2017.

- [33] Doyeon Kim, Woonghyun Ga, Pyungwhan Ahn, Donggyu Joo, Sehwan Chun, and Junmo Kim. Global-local path networks for monocular depth estimation with vertical cutdepth. *arXiv*, 2022.
- [34] Seungryong Kim, Kihong Park, Kwanghoon Sohn, and Stephen Lin. Unified depth prediction and intrinsic image decomposition from a single image via joint convolutional neural fields. In *ECCV*, pages 143–159, 2016.
- [35] Solomon Kullback. *Information theory and statistics*. Courier Corporation, 1997.
- [36] Varun Ravi Kumar, Sandesh Athni Hiremath, Markus Bach, Stefan Milz, Christian Witt, Clément Pinard, Senthil Yogamani, and Patrick Mäder. Fisheyedistancenet: Self-supervised scale-aware distance estimation using monocular fisheye camera for autonomous driving. In *ICRA*, pages 574–581. IEEE, 2020.
- [37] Jogendra Nath Kundu, Phani Krishna Uppala, Anuj Pahuja, and R Venkatesh Babu. Adadepth: Unsupervised content congruent adaptation for depth estimation. In *Proceedings of the IEEE conference on computer vision and pattern recognition*, pages 2656–2665, 2018.
- [38] Yevhen Kuznietsov, Jorg Stuckler, and Bastian Leibe. Semi-supervised deep learning for monocular depth map prediction. In *CVPR*, pages 6647–6655, 2017.
- [39] Lubor Ladicky, Jianbo Shi, and Marc Pollefeys. Pulling things out of perspective. In *CVPR*, pages 89–96, 2014.
- [40] Jin Han Lee, Myung-Kyu Han, Dong Wook Ko, and Il Hong Suh. From big to small: Multi-scale local planar guidance for monocular depth estimation. *arXiv*, 2019.
- [41] Wonwoo Lee, Nohyoung Park, and Woontack Woo. Depth-assisted real-time 3d object detection for augmented reality. In *ICAT*, volume 11, pages 126–132, 2011.
- [42] Bo Li, Chunhua Shen, Yuchao Dai, Anton Van Den Hengel, and Mingyi He. Depth and surface normal estimation from monocular images using regression on deep features and hierarchical crfs. In *CVPR*, pages 1119–1127, 2015.
- [43] Zhenyu Li, Zehui Chen, Xianming Liu, and Junjun Jiang. Depthformer: Exploiting long-range correlation and local information for accurate monocular depth estimation. *arXiv*, 2022.
- [44] Fayao Liu, Chunhua Shen, Guosheng Lin, and Ian Reid. Learning depth from single monocular images using deep convolutional neural fields. *PAMI*, 38(10):2024–2039, 2015.
- [45] Nikolaus Mayer, Eddy Ilg, Philip Hausser, Philipp Fischer, Daniel Cremers, Alexey Dosovitskiy, and Thomas Brox. A large dataset to train convolutional networks for disparity, optical flow, and scene flow estimation. In *CVPR*, pages 4040–4048, 2016.
- [46] Luke Melas-Kyriazi and Arjun K Manrai. Pixmatch: Unsupervised domain adaptation via pixelwise consistency training. In *Proceedings of the IEEE/CVF Conference on Computer Vision and Pattern Recognition*, pages 12435–12445, 2021.
- [47] Adam Paszke, Sam Gross, Soumith Chintala, Gregory Chanan, Edward Yang, Zachary DeVito, Zeming Lin, Alban Desmaison, Luca Antiga, and Adam Lerer. Automatic differentiation in pytorch. 2017.
- [48] Deepak Pathak, Philipp Krahenbuhl, Jeff Donahue, Trevor Darrell, and Alexei A Efros. Context encoders: Feature learning by inpainting. In *CVPR*, pages 2536–2544, 2016.
- [49] Koutilya PNVR, Hao Zhou, and David Jacobs. Sharingan: Combining synthetic and real data for unsupervised geometry estimation. In *Proceedings of the IEEE/CVF Conference on Computer Vision and Pattern Recognition*, pages 13974–13983, 2020.
- [50] Matteo Poggi, Filippo Aleotti, Fabio Tosi, and Stefano Mattoccia. On the uncertainty of self-supervised monocular depth estimation. In *CVPR*, pages 3227–3237, 2020.
- [51] René Ranftl, Alexey Bochkovskiy, and Vladlen Koltun. Vision transformers for dense prediction. In *ICCV*, pages 12179–12188, 2021.
- [52] René Ranftl, Katrin Lasinger, David Hafner, Konrad Schindler, and Vladlen Koltun. Towards robust monocular depth estimation: Mixing datasets for zero-shot cross-dataset transfer. *PAMI*, 2020.
- [53] Ashutosh Saxena, Sung H Chung, and Andrew Y Ng. 3-d depth reconstruction from a single still image. *IJCV*, 76(1):53–69, 2008.
- [54] Nathan Silberman, Derek Hoiem, Pushmeet Kohli, and Rob Fergus. Indoor segmentation and support inference from rgbd images. In *ECCV*, pages 746–760. Springer, 2012.
- [55] Kihyuk Sohn, David Berthelot, Nicholas Carlini, Zizhao Zhang, Han Zhang, Colin A Raffel, Ekin Dogus Cubuk, Alexey Kurakin, and Chun-Liang Li. Fixmatch: Simplifying semi-supervised learning with consistency and confidence. *NIPS*, 33:596–608, 2020.
- [56] Shuran Song, Samuel P Lichtenberg, and Jianxiong Xiao. Sun rgb-d: A rgb-d scene understanding benchmark suite. In *Proceedings of the IEEE conference on computer vision and pattern recognition*, pages 567–576, 2015.
- [57] Alessio Tonioni, Matteo Poggi, Stefano Mattoccia, and Luigi Di Stefano. Unsupervised domain adaptation for depth prediction from images. *PAMI*, 42(10):2396–2409, 2019.
- [58] Fabio Tosi, Filippo Aleotti, Matteo Poggi, and Stefano Mattoccia. Learning monocular depth estimation infusing traditional stereo knowledge. In *CVPR*, pages 9799–9809, 2019.
- [59] Jonas Uhrig, Nick Schneider, Lukas Schneider, Uwe Franke, Thomas Brox, and Andreas Geiger. Sparsity invariant cnns. In *3DV*, pages 11–20. IEEE, 2017.
- [60] Benjamin Ummenhofer, Huizhong Zhou, Jonas Uhrig, Nikolaus Mayer, Eddy Ilg, Alexey Dosovitskiy, and Thomas Brox. Demon: Depth and motion network for learning monocular stereo. In *CVPR*, pages 5038–5047, 2017.
- [61] Xiaolong Wang, David Fouhey, and Abhinav Gupta. Designing deep networks for surface normal estimation. In *CVPR*, pages 539–547, 2015.
- [62] Zhou Wang and Alan C Bovik. Mean squared error: Love it or leave it? a new look at signal fidelity measures. *IEEE signal processing magazine*, 26(1):98–117, 2009.
- [63] Jamie Watson, Michael Firman, Gabriel J Brostow, and Daniyar Turmukhambetov. Self-supervised monocular depth hints. In *ICCV*, pages 2162–2171, 2019.
- [64] Jamie Watson, Oisín Mac Aodha, Victor Prisacariu, Gabriel Brostow, and Michael Firman. The temporal opportunist:

- Self-supervised multi-frame monocular depth. In *Proceedings of the IEEE/CVF Conference on Computer Vision and Pattern Recognition*, pages 1164–1174, 2021.
- [65] Junyuan Xie, Ross Girshick, and Ali Farhadi. Deep3d: Fully automatic 2d-to-3d video conversion with deep convolutional neural networks. In *ECCV*, pages 842–857. Springer, 2016.
  - [66] Zhenda Xie, Zheng Zhang, Yue Cao, Yutong Lin, Jianmin Bao, Zhuliang Yao, Qi Dai, and Han Hu. Simmim: A simple framework for masked image modeling. *arXiv*, 2021.
  - [67] Haohang Xu, Shuangrui Ding, Xiaopeng Zhang, Hongkai Xiong, and Qi Tian. Masked autoencoders are robust data augmentors. *arXiv preprint arXiv:2206.04846*, 2022.
  - [68] Guanglei Yang, Hao Tang, Mingli Ding, Nicu Sebe, and Elisa Ricci. Transformer-based attention networks for continuous pixel-wise prediction. In *ICCV*, pages 16269–16279, 2021.
  - [69] Wei Yin, Yifan Liu, Chunhua Shen, and Youliang Yan. Enforcing geometric constraints of virtual normal for depth prediction. In *Proceedings of the IEEE/CVF International Conference on Computer Vision*, pages 5684–5693, 2019.
  - [70] Senthil Yogamani, Ciarán Hughes, Jonathan Horgan, Ganesh Sistu, Padraig Varley, Derek O’Dea, Michal Uricár, Stefan Milz, Martin Simon, Karl Amende, et al. Woodscape: A multi-task, multi-camera fisheye dataset for autonomous driving. In *Proceedings of the IEEE/CVF International Conference on Computer Vision*, pages 9308–9318, 2019.
  - [71] Chaoning Zhang, Kang Zhang, Chenshuang Zhang, Trung X Pham, Chang D Yoo, and In So Kweon. How does sim-siam avoid collapse without negative samples? a unified understanding with self-supervised contrastive learning. *arXiv*, 2022.
  - [72] Shanshan Zhao, Huan Fu, Mingming Gong, and Dacheng Tao. Geometry-aware symmetric domain adaptation for monocular depth estimation. In *Proceedings of the IEEE/CVF Conference on Computer Vision and Pattern Recognition*, pages 9788–9798, 2019.
  - [73] Chuanxia Zheng, Tat-Jen Cham, and Jianfei Cai. T2net: Synthetic-to-realistic translation for solving single-image depth estimation tasks. In *Proceedings of the European Conference on Computer Vision (ECCV)*, pages 767–783, 2018.
  - [74] Tinghui Zhou, Matthew Brown, Noah Snavely, and David G Lowe. Unsupervised learning of depth and ego-motion from video. In *CVPR*, pages 1851–1858, 2017.
  - [75] Yuliang Zou, Zizhao Zhang, Han Zhang, Chun-Liang Li, Xiao Bian, Jia-Bin Huang, and Tomas Pfister. Pseudoseg: Designing pseudo labels for semantic segmentation. *arXiv*, 2020.